

A method for statistical research on binary stars using radial velocities

LUO FENG,^{1,2,3} ZHAO, YONG HENG,^{2,3} AND LIU CHAO^{2,3}

¹*Institute of Physics, Chinese Academy of Sciences, Beijing 100080, China*

²*National Astronomical Observatories, Chinese Academy of Sciences, Beijing 100012, China*

³*University of Chinese Academy of Sciences, Beijing 100049, China*

ABSTRACT

Using radial velocity to estimate binary fraction and predict orbital parameter distribution laws is an important method in the studies of binary stars. However, the high dimensionality of the orbital parameters of the binary system pose challenges to this work, particularly in terms of sample size and the accuracy of the calculated results.

We have proposed and implemented an algorithm called DVCD (Differential Velocity Cumulative Distribution) for the statistical analysis of binary properties. This method not only achieves higher accuracy than previous approaches but also significantly improves computational efficiency. The computing time for the same sample and the hardware environment was reduced to 10^{-4} to 10^{-5} of that of some previous methods.

Red giant samples from APOGEE DR16 were analyzed using the DVCD method. Both the hyperparameter of the orbital period π and the intrinsic binary fraction (f_{bin}) can be constrained. We divided the sample into 16 subsets based on $\log g$ and M/H . Calculation results showed that the binary fraction decreases with the decrease of surface gravity and decreases with the increase of metallicity. This trend provides important constraints on the evolution of binary stars.

Keywords: Binary (251) — Algorithm (1736) — Red giants(1868)

1. INTRODUCTION

Binary stars are very important objects of study in astronomy and astrophysics. The interactions between two member stars in close binary systems provide much information to research their properties (van Kooten et al. 2020; Mazzola et al. 2020; Gies et al. 2020; Ge et al. 2015; Khoshnood et al. 2015; Kangas et al. 2017; Lomax et al. 2017; Peters 2011). There are abundant astronomical phenomena in some binary star systems with dense star members, such as X-ray binaries (Karino 2022; García et al. 2022; Zhang et al. 2022; Wang et al. 2022), supernovae (Blondin et al. 2021; Shin et al. 2021; Shao & Li 2018; Ziegerer et al. 2017; Saz Parkinson et al.

2016; Tsebrenko & Soker 2015), kilonovae (Dubey & Pathak 2021; Callister 2021) and so on. The extreme physical conditions of these binary systems, such as high temperatures, strong magnetism, and strong gravitational fields, provide ideal natural laboratories for testing basic physical theories. For example, the widely concerned event GW150914 was the first time that humans directly observed gravitational waves, which are caused by the merger of a black hole binary system (Shapiro 2016; Spera et al. 2016; Lynch et al. 2015). It not only provides strong evidence for general relativity, but also tests Hawking’s black hole area theorem (Isi et al. 2021).

Through the Doppler effect of electromagnetic waves, radial velocities of stars can be derived from spectroscopic analysis. It can provide us with much useful information about the state of motion of celestial bodies. This method is widely used in sky survey research (Zheng & Shen 2021; Liao et al. 2021; Zheng & Shen 2020a,b; Lu et al. 2019, 2018; Lee & Lin 2017). Because of orbital motion, radial velocities of the components in binary systems would present periodic changes. And different orbital parameters, such as orbital periods, primary masses, eccentricities, and inclinations, correspond to different variations. The more sufficient the observations are, the more likely it is for us to obtain these parameters. However, in numerous instances, we lack enough observational data to accurately acquire all of these parameters (Table 1). Instead, we are able to study them from a statistical point of view.

The statistical properties of binaries can bring us some references to infer the evolution of single stars, binaries, and even galaxies. Binary fractions of different samples were paid much attention in recent years (Raghavan et al. 2010; Chini et al. 2012,?; Sana et al. 2012; Sota et al. 2014; Kobulnicky et al. 2014; Dunstall et al. 2015; Al-doretta et al. 2015). However, the distribution laws of orbital parameters such as orbital periods, mass ratios, eccentricities, etc., are not well known (Sana et al. 2013; Gao et al. 2014, 2017; Tian et al. 2018; Guo et al. 2021; Luo et al. 2021). On one hand, the raw observation data are limited. On the other hand, the existing methods face different problems which could lead to a declination in the accuracy of the final results. In this research, we propose a new method for estimating the intrinsic binary fraction (f_{bin}) and predicting the distributions of the orbital parameters. Experiments show that this method has high accuracy and efficiency.

This article is organized in the following way. A brief introduction is given in Sect.1. Some difficulties of previous methods were analyzed in Sect.2. The new method for statistical research on binaries using radial velocities was elaborated in Sect.3. The scientific application for observational data from APOGEE DR16 was demonstrated in Sect.4. The discussion and conclusion are described in Sect.5.

2. PREVIOUS METHODS

There are 7 parameters that determine the orbital phases of radial velocities, see Table 1. Then the RV Equation.1 can be drawn through Kepler’s laws and elliptical geometric calculation Hilditch (2001).

Name	Comment
P	orbital period
q	mass ratio
e	eccentricity
m_1	mass of the primary
i	angle of inclination
ω	longitude of the periastron
T_0	the time of periastron passage

Table 1. Kinematics orbital parameters of binary

$$\begin{aligned}
 \text{RV} &= \frac{2\pi a_1 \sin i}{P\sqrt{(1-e^2)}} [\cos(\theta + \omega) + e \cos \omega] + \gamma, \\
 a_1 &= \frac{a}{(1+q)}, \quad a = \left(\frac{Gm_1(1+q)P^2}{4\pi^2} \right)^{\frac{1}{3}}, \\
 \theta &= \cos^{-1} \left(\frac{\cos E - e}{1 - e \cos E} \right), \quad E - e \sin E = 2\pi \frac{t - T_0}{P}.
 \end{aligned} \tag{1}$$

Here γ is the systemic velocity or the radial velocity of the center of mass of the binary system. It relates to the motion of the whole system. a_1 is the long axis of the elliptic orbit of the primary, which is associated with the mass ratio q . θ is the position angle between the radius vector and a reference direction, which is a function of the time of an observational epoch. P , e , i , ω and T_0 are orbital period, eccentricity, angle of inclination, precession angle and the time of periastron passage. Thus, we can get a simulated RV by given a set of the 7 orbital parameters and an observational time.

The existing methods for statistical research on binary characteristics mainly contain two kinds. The Hierarchical Bayesian Model (HBM) and the algorithm proposed by Sana et al. (2013) (S13, hereafter). The main equation Liu et al. (2014); Gao et al. (2017); Tian et al. (2018) of HBM is

$$p(\Delta RV) = f_B p_B(\Delta RV | \sigma_{RV}, \Delta t, M_B) + (1 - f_B) p_S(\Delta RV | \sigma_{RV}) \tag{2}$$

where f_B is the binary fraction, σ_{RV} the measurement error of radial velocities. Δt represent the time interval between two observational epochs. $p_B(\Delta RV | \sigma_{RV}, \Delta t, M_B)$ and $p_S(\Delta RV | \sigma_{RV})$ denote probabilities of obtaining ΔRV under the assumptions of binaries and single stars, respectively Tian et al. (2018). M_B is a binary model to draw simulated RVs containing all orbital parameters and possible hyper-parameters.

Main equations of the S13 method are:

$$\frac{|v_i - v_j|}{\sqrt{\varepsilon_i^2 + \varepsilon_j^2}} > a (a = 4.0) \quad \text{and} \quad |v_i - v_j| > C (C = 20 \text{ km s}^{-1}), \tag{3}$$

$$\Xi' = P_{\text{KS}}(\Delta RV) \times P_{\text{KS}}(\Delta HJD) \times B(N_{\text{bin}}, N, f_{\text{bin}}^{\text{simul}}) \tag{4}$$

A global merit function (Ξ') is constructed by multiplying the two KS probabilities obtained for the ΔRV and ΔHJD distributions and the Binomial probability. Where ΔRV are those satisfying Equation.(3) and ΔHJD are the corresponding observational interval. f_{bin}^{simul} is the binary fraction detected in simulated samples, N_{bin} the number of binaries detected in observational data by Equation.3. N is the sample size.

The HBM is to investigate and explore the behavior of $P(\Delta RV)$ in the parameter space, while S13 method is of Ξ' . Beside the binary fraction we also intend to know the distributions of orbital parameters such as P , q , and e . Following S13 we generally assumed P , q , and e obey power law distributions with exponents π , κ and η as Equation.5.

$$f(P) \sim P^\pi, f(q) \sim q^\kappa, f(e) \sim e^\eta. \quad (5)$$

In some cases we need to define the mean measurement error of RV as ε to investigate the affects of final results caused by different RV uncertainties. Normally there are at least 8 dimensions like $(P, q, e, m_1, i, \omega, T_0, f_{bin})$. Number of dimensions will achieve 12 if we consider the hyper-parameters and ε , $(P, q, e, m_1, i, \omega, T_0, f_{bin}, \pi, \kappa, \eta, \varepsilon)$.

Both of these two methods calculate samples one by one in the multi-dimensional parameter space. In order to get more reliable results we must draw samples as completely as possible. From simulated experiments with the 2 methods carried out by us in the past years we found the following facts. When sample size is small (< 200) and with fewer epochs (2, 3, 4) the analysis results are not reliable and unrepresentative. As the number of samples and epochs increase the computation will be more and more time consuming. If sampling is reduced to shorten the running time, the final analysis results will be affected by large statistical fluctuations.

In the statistical research on binary properties through spectroscopic approaches, what data we have are observational epochs RV and the corresponding radial velocities. The majority of existing methods are based on single statistical magnitude of RV like σ_{RV} Tian et al. (2018), or ΔRV s which show obvious variation of any pairs of RV within the several repeated observations (S13).

σ_{RV} can reflect the degree of dispersion of RVs, however, probably loses the information of orbital parameters. It can be used to estimate the f_{bin} but is difficult to predict the orbital parameters and, further more, the distribution laws of orbital parameters. ΔRV s that respect evidently change of any pairs of observed RVs faced two hidden problems. Firstly, determining the threshold to judge the significance of the RV changes is easy to be subjectively. The threshold is 4 (Equation.3) in (S13), which will causes a difference nearly 0.5 between the detected spectroscopic binary fraction and f_{bin} in some cases. Secondly, due to the existence of measurement error, ΔRV that change remarkably of single stars, often the ΔRV_{max} , will behave more and more like a binary as the number of observational epochs increase.

3. THE DVCD ALGORITHM

3.1. Difference sequences of RVs

In view of the above situation, we make improvements and propose a new algorithm. The above-mentioned difficulties can be solved by using the difference sequences (DS) of RVs in chronological order as basic observational data. First, it deducts the systemic velocities by subtraction. Then, it largely retains the raw data and the underlying orbital parameter information.

The elements in DS of RVs defined as $\Delta AJRV$ (adjacent RV):

$$\Delta AJRV_j = RV_k - RV_j, \quad (j = 1, 2, 3, \dots, n-1; k = j+1), \quad (6)$$

where n is the number of observations. To check the validity of $\Delta AJRV$, we can construct a likelihood function (Equation.7) using $\Delta AJRV$ to estimate the orbital parameters of a single sample. Where N is the probability distribution function of the normal distribution. The term sub-scripted *simul* is the simulated data generated by RV Equation 1, while the term sub-scripted *obs* is derived from the observational RVs. Suppose that the RV measurement error follows the normal distribution $N(0, \varepsilon)$. From probability theory, $\Delta AJRV$ should satisfy the distribution $N(0, \sqrt{2}\varepsilon)$.

$$\begin{aligned} L(\theta^* | \Delta AJRV) &= \prod_1^{n-1} f(\Delta AJRV_j | \theta^*), \\ f(\Delta AJRV_j | \theta^*) &= N(\Delta AJRV_{j_{simul}}, \mu = \Delta AJRV_{j_{obs}}, \sigma = \sqrt{2}\varepsilon), \\ \theta^* &= (P, q, e, m_1, i, \omega, T_0) \end{aligned} \quad (7)$$

We generated a mock binary orbit sample with $\theta^* = 300, 0.7, 0.4, 6, \pi/3, \pi/6, 90$ and evenly sampled the RV 20 times. The detection ranges of parameters in this experiment are defined in Table 2. The calculated results by use of the emcee program package in Python were shown in Figure 1. To make the picture clearer, we have removed data with likelihood probabilities less than the 10th quantile. We can see that the orbital period P and eccentricity e were well constrained in narrow ranges. Although true values of mass ratio q and primary mass m_1 were contained in their corresponding results, the error ranges of them are wider than P or e . That's because there is degeneracy between q and m_1 in radial velocities.

The angle of inclination i , angle of precession ω , and the time of periastron passage T_0 are not intrinsic properties of binary orbits. They depend on the relative position of the binary system and the observer. For the most part, we care more about the other parameters P, q, e and m_1 . Figure 1 shows it is feasible to use DS to estimate the orbital parameters for a given binary.

3.2. Cumulative distribution characteristics of DS of RVs

The cumulative distribution curve (CDC) implies the distribution characteristics of a group of data. The curve shape, definition domain, inflection point position,

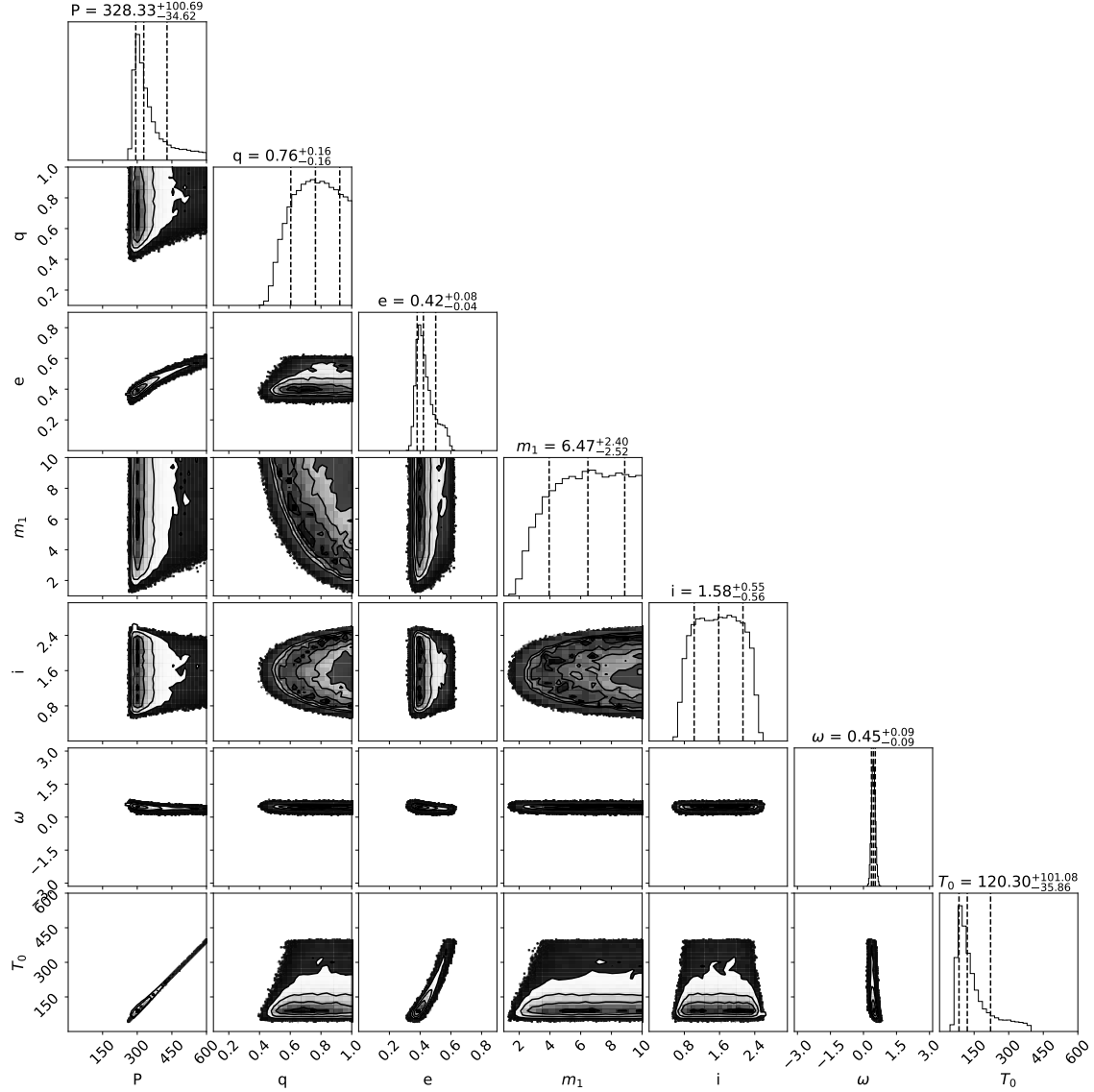


Figure 1. Result of the prediction of orbital parameters using the MCMC approach. The black dashed lines in each 1d subgraph respectively indicate the position of the 15th, 50th, and 85th percentiles.

Table 2. Detection ranges of orbital parameters.

Name	$P(\text{day})$	q	e	$m_1(M_\odot)$	i	ω	T_0
Range	[1, 600]	[0.1, 1]	[0, 0.9]	[1, 10]	[0, π]	$[-\pi, +\pi]$	[0, P]

and slope at the inflection point, and so on, of different data are different. These properties make it possible to predict the f_{bin} and the distribution laws of orbital parameters.

Before we do experiments, some conventions about symbols and assumptions should be made.

Table 3. The true values of orbital parameters in this experiment.

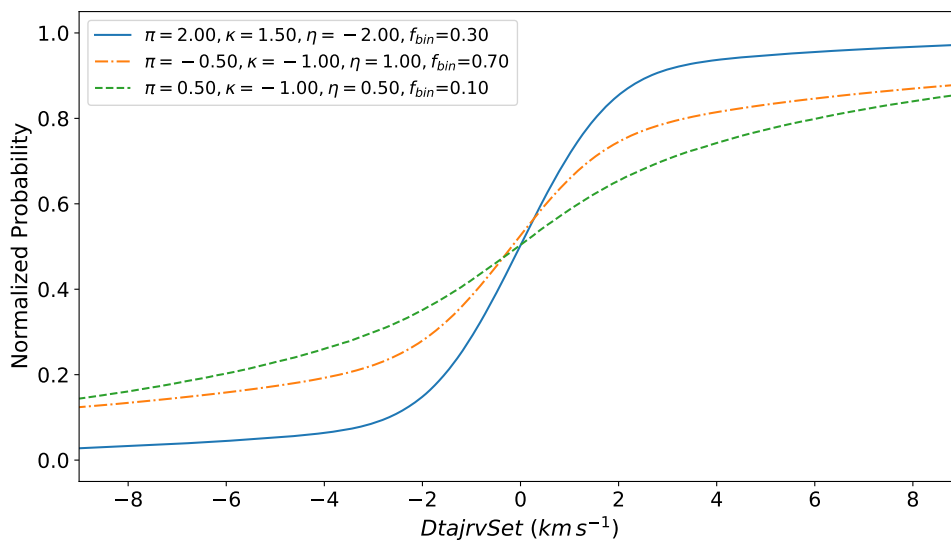
π	κ	η	f_{bin}
2.0	1.5	-2.0	0.3
-0.5	-1	1.0	0.7
0.5	-1	0.5	0.1

1). Each group contained 10^5 observational sources in the simulation data to construct the CDC. Each source has 11 repeated observations.

2). The set of $\Delta AJRV$ sequences of all the samples is called *DtajrvSet*.

3). It is assumed that the orbital period P , mass ratio q and eccentricity e obey power law distributions with power exponents π , κ and η , respectively (Equation 5).

We generate 3 groups of mock samples, the parameters of them are described in Table 3. The CDCs of these 3 groups are shown in Figure 2, from which we can see that all 3 curves are different from each other, which means they carry their own parameter information. In other words, the distribution characteristics of the orbital parameters were successfully encoded in the CDCs.


Figure 2. The difference of the cumulative distribution curves of *DtajrvSet* of binary star samples generated with different π , κ , η and f_{bin} . In this figure the $\varepsilon = 1.0 \text{ km s}^{-1}$

3.3. Implementation of the DVCD method

The key to algorithmic implementation is how to judge whether two samples are from the same distribution, or the degree of similarity of distributions between two samples. KS test is used to judge the correlation between two samples by comparing their CDCs. The *Pvalue* given by the KS test represents the degree of correlation of two samples, the larger the *Pvalue*, the higher the consistency.

For real observational data, generating simulation data at the scale of real data often fails to construct a smooth enough CDC due to insufficient random sampling.

If different parameters are generated in real-time during the operation, and the data are fully sampled for comparison, the calculation cost will be immeasurable. To this end, we adopt the strategy of “space for time” to generate simulation samples under different conditions in advance and assemble their $\Delta AJRV$ s into $DtajrvSet$ as the “basic template library”. We simply need to read out the “basic template” of different parameters and compare them with the data we want to measure. Then, we can use the KS test to obtain the corresponding $Pvalue$. This way can greatly reduce the running time of the program. In our experiments, each “basic template” contains 10^6 $\Delta AJRV$. For example, take 11 times for each orbit we generate 10^5 orbits under a combination of $(\pi, \kappa, \eta, \varepsilon)$.

During the comparison process between the data to be measured and the “templates”, a temporary “mixed $DtajrvSet$ ” was formed by sampling $\Delta AJRV$ in the ratio of f_{bin} to $(1 - f_{bin})$ from $DtajrvSet$ of binary and single stars. In the execution of the algorithm, the f_{bin} was traversed from 0.0 to 1.0 with a step size of 0.01. This procedure can be written as Equation 8.

$$Pvalue(\pi, \kappa, \eta, \varepsilon, f_{bin}) = P_{KS}(DtajrvSet_{obs}, DtajrvSet_{tmpl}(\pi, \kappa, \eta, \varepsilon, f_{bin})) \quad (8)$$

Then we can study the binary characteristics by analyzing the performance of $Pvalue$ in the parameter space.

3.4. Validations with mock data

Two groups of samples were generated with a sample size equal to 1000, epochs 11, $\varepsilon = 1.0 \text{ km s}^{-1}$, true $f_{bin} = 0.5$, $\kappa, \eta = (0, 0)$ but different $\pi = (-1.5, 0.5)$. The ranges of values for the orbital parameters except P and e are shown in Table 2. The upper limit of P was set to 3000 to contain systems which have longer orbital periods, and the minimum value range of e was set to 10^{-5} to avoid the exception with a zero divisor. The parameters m_1, i, ω, T_0 are assumed to follow uniform distributions. The calculated results using the DVCD algorithm of the two groups were shown in Figure 3 and Figure 4, respectively. From the two graphics, we can see that the truths of both π and f_{bin} can be restored accurately.

Furthermore, we generate a group of samples with true $(\pi, \kappa, \eta, f_{bin}) = (-1.6, 0.8, -1.4, 0.3)$ to test if the truths can be restored. The results are displayed in Figure 5. It can be seen that π and f_{bin} were well constrained, while the error range of κ and η is wider than π . Two reasons may cause this phenomenon. On the one hand, the sample size 1000 and true $f_{bin} = 0.3$ mean that there are few binaries that carry orbital information to predict the distribution laws of κ and η . On the other hand, the prior distributions of q and e do not significantly affect $DtajrvSet$ more than π and f_{bin} . Generally speaking, the accuracy of the estimates of f_{bin} was better than π, κ , and η .

Some relatively sparsely generated data were used to explore the algorithmic performance. Two data sets with the same sample size 200 and true value of

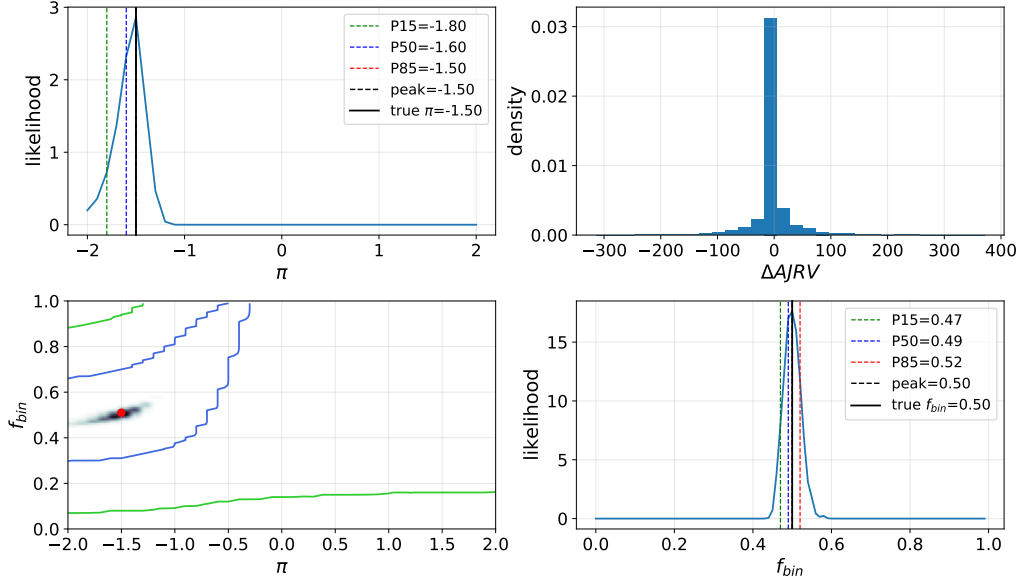


Figure 3. Calculated results of samples whose π equals -1.5 , the black solid lines in the graph represent the position of true values. Red point indicated the peak position.

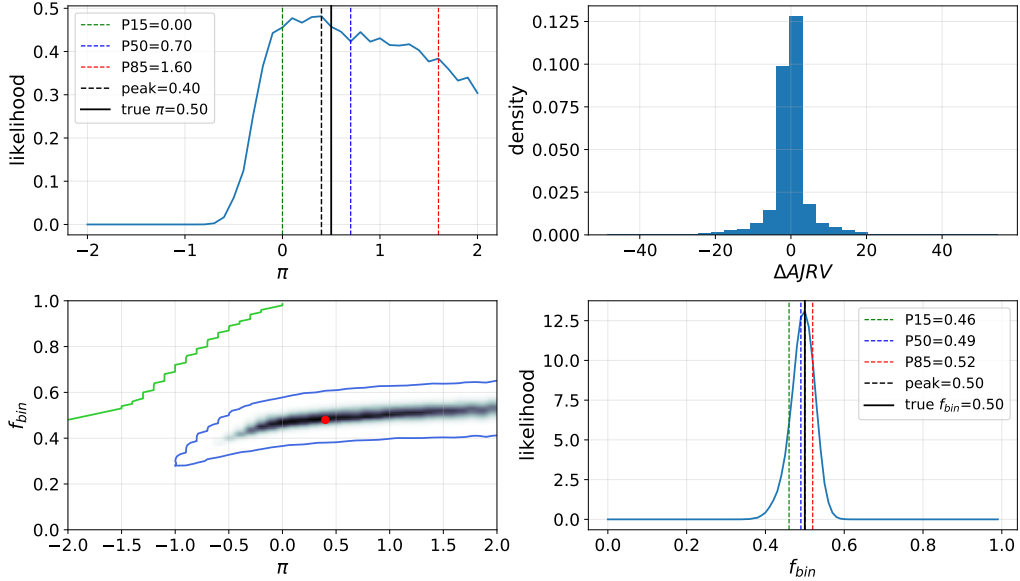


Figure 4. Calculated results of samples whose π equals 0.5 , the black solid lines in the graph represent the position of true values. Red point indicated the peak position.

$(\pi, \varepsilon) = (-1.5, 1.0)$ were created. The true f_{bin} of the first data set is 0.4 . We varied epochs from 2 to 25 to observe the estimations of π and f_{bin} as shown in Figure 6. It can be seen that the error of f_{bin} and π are large when number of epochs is 2. The both error margins were getting shorter when epochs increase especially the f_{bin} ; Observational epochs of the second data set is 10. The true f_{bin} was altered from 0.1 to 0.9 . It was found that π was not well constrained when $f_{bin} = 0.1$. That is because there are only 20 binaries and they can not provide sufficient orbital information.

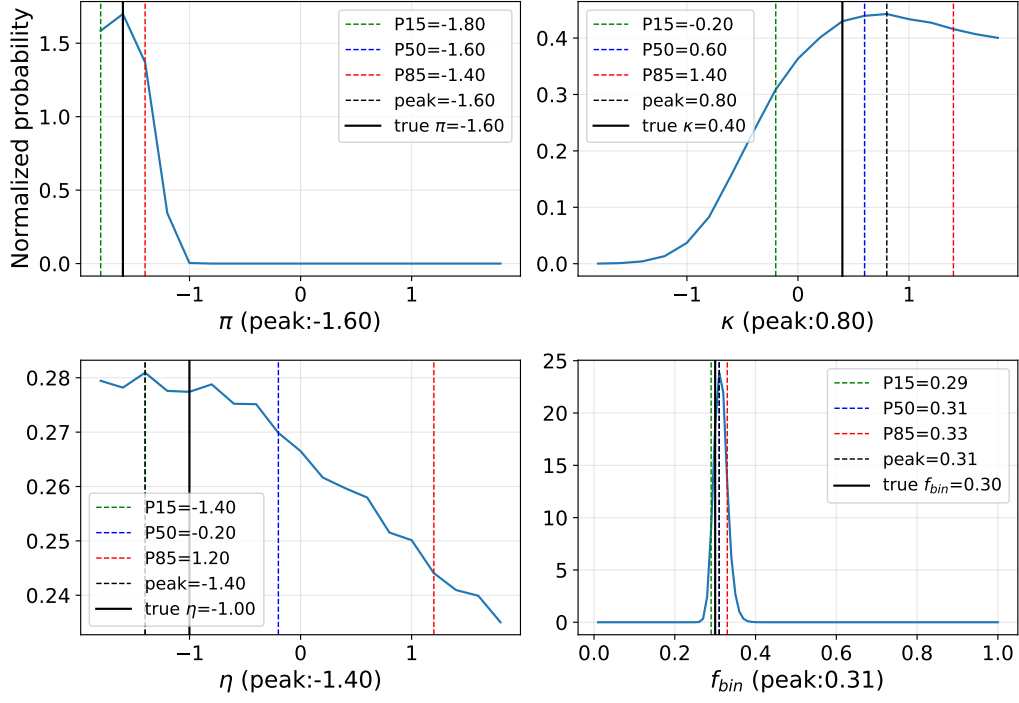


Figure 5. The difference of the cumulative distribution curves of *DtajrvSet* of binary star samples generated with different π , κ , η and f_{bin} . In this figure the $\varepsilon = 1.0 \text{ km s}^{-1}$

This fact also implies that the predictions of orbital parameters would not be reliable when the calculated f_{bin} was small, particularly close to 0.1.

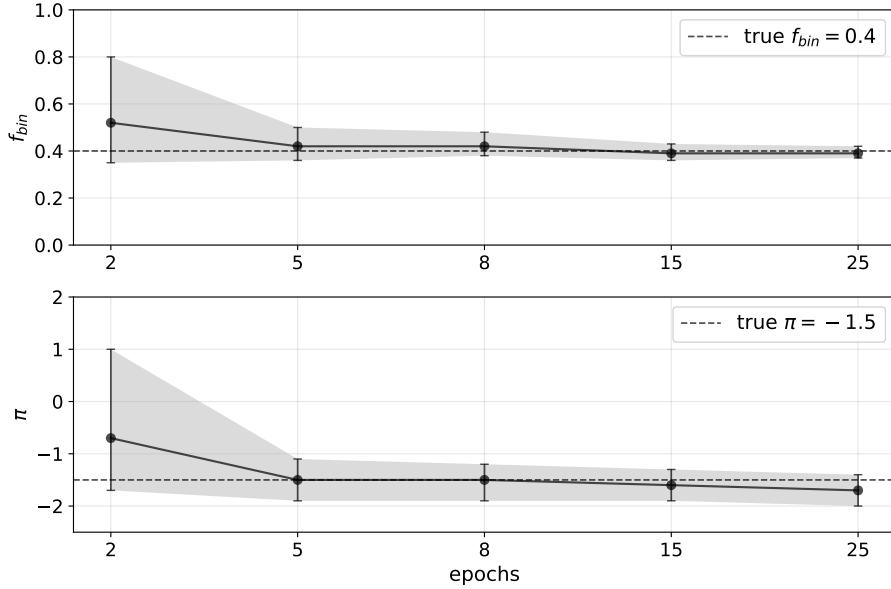


Figure 6.

4. SCIENTIFIC APPLICATION

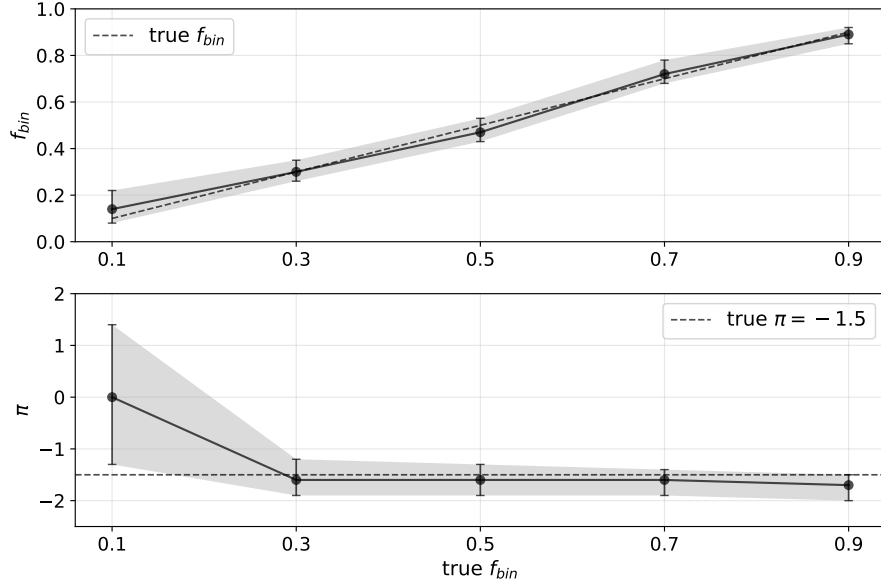


Figure 7.

4.1. Red giant samples from APOGEE DR16

We used data of red giant stars selected from APOGEE DR16 to test the algorithm. Liu et al. (2014) presents a simple strategy for preliminary selection of red giants by T_{eff} and $\log g$. The regions are considered to have better red giant completeness where $\log g < 4$ when $4600 < T_{eff} < 5600$ or $\log g < 3.5$ when $T_{eff} < 4600$. It needs to be pointed out that there are spectra containing bad pixels or with low SNR included in the star catalogue released by APOGEE. Therefore, we should pay attention to the markers in the catalogue Price-Whelan et al. (2018); Troup et al. (2016). Our data filtering criteria mainly included the following:

- 1). $SNR \geq 20$;
- 2). There are at least 6 repeated observations;
- 3). $\log g < 4$ when $4600 < T_{eff} < 5600$ or $\log g < 3.5$ when $T_{eff} < 4600$;
- 4). Remove spectra satisfying: In ‘‘APOGEE_STARFLAG’’ field, the ‘‘LOW_SNR’’, ‘‘VERY_BRIGHT_NEIGHBOR’’, ‘‘PERSIST_JUMP_NEG’’, ‘‘PERSIST_JUMP_POS’’, ‘‘BAD_PIXELS’’, ‘‘PERSIST_HIGH’’ markers equal to 1. In ‘‘APOGEE_ASPCAPFLAG’’ field the ‘‘STAR_BAD’’ marker equals to 1.

15182 sources were sought out, then we eliminated some abnormal data at the lower right dotted line in Figure 8 and 15112 were left. The basic information of them was depicted in Figure 9. Where the observational intervals are time intervals between any pairs of observations.

4.2. Mean measurement error of RVs

A simple test was carried out to roughly estimate the spectroscopic binary fraction by using the first equation of Equation.3. Here v_i and ε_i are the RV and the RV error at epoch i for a given observational source.

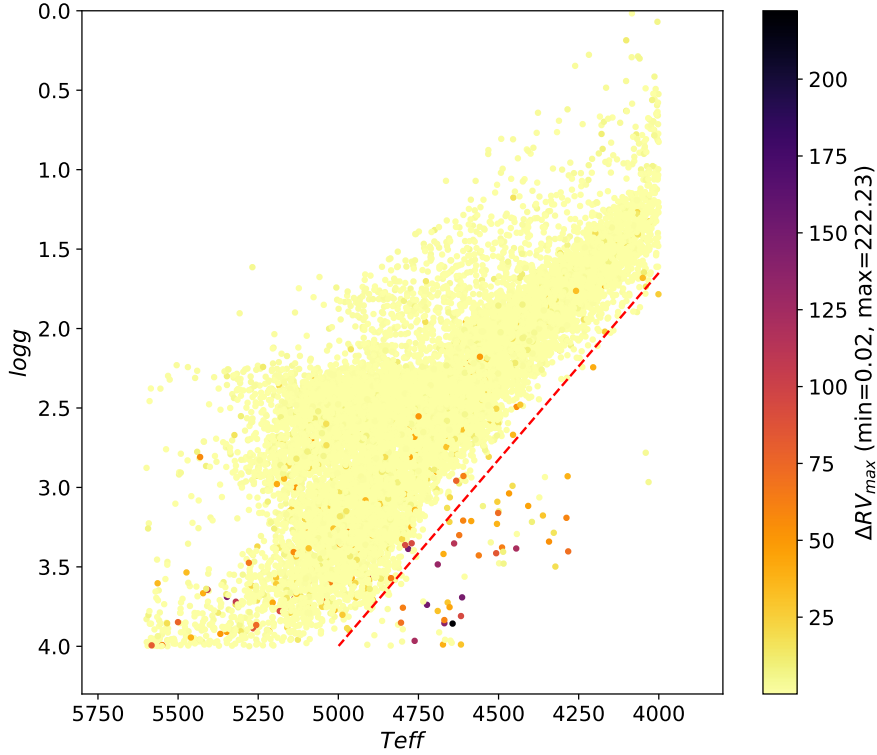


Figure 8. Red giant samples from APOGEE DR16.

We changed a from 1.0 to 6.0 with step 0.5 and recorded the corresponding binary fraction, as shown in Figure 10. The directly detected f_{bin} can be seen in the figure was exceeded by 0.9 when $a = 3.0$, which seems to be a little high. As summarized in Luo et al. (2021), most main-sequence stars do not have a so high f_{bin} . Therefore, the RV measurement error provided by the APOGEE DR16 catalogue may be underestimated. We need to reassess the RV measurement error of these samples.

It is assumed that the left part of the ΔRV_{max} distribution curve from observational data was contributed by single stars. We generated single star samples with different mean measurement error of RV ε . The parts to the left of the observed peak of these samples were intercepted to compare with the corresponding observed curve utilizing the least square approach. The minimum of least square was emerged when $\varepsilon = 0.074$. Then we adopted 0.074 km s^{-1} as the uniform RV measurement error of all observational samples.

4.3. Lower limits of orbital period detection

We divided the samples into 16 parts according to M/H and $\log g$, see Figure 11. Samples whose $2.2 < \log g < 2.8$ were not included in since this area may contain many red clumps. Considering that the radii of red giants with different $\log g$ vary greatly and the orbital periods are related to the separations between the two components in a binary system. We do sketchy estimations of the minima of orbital period detection

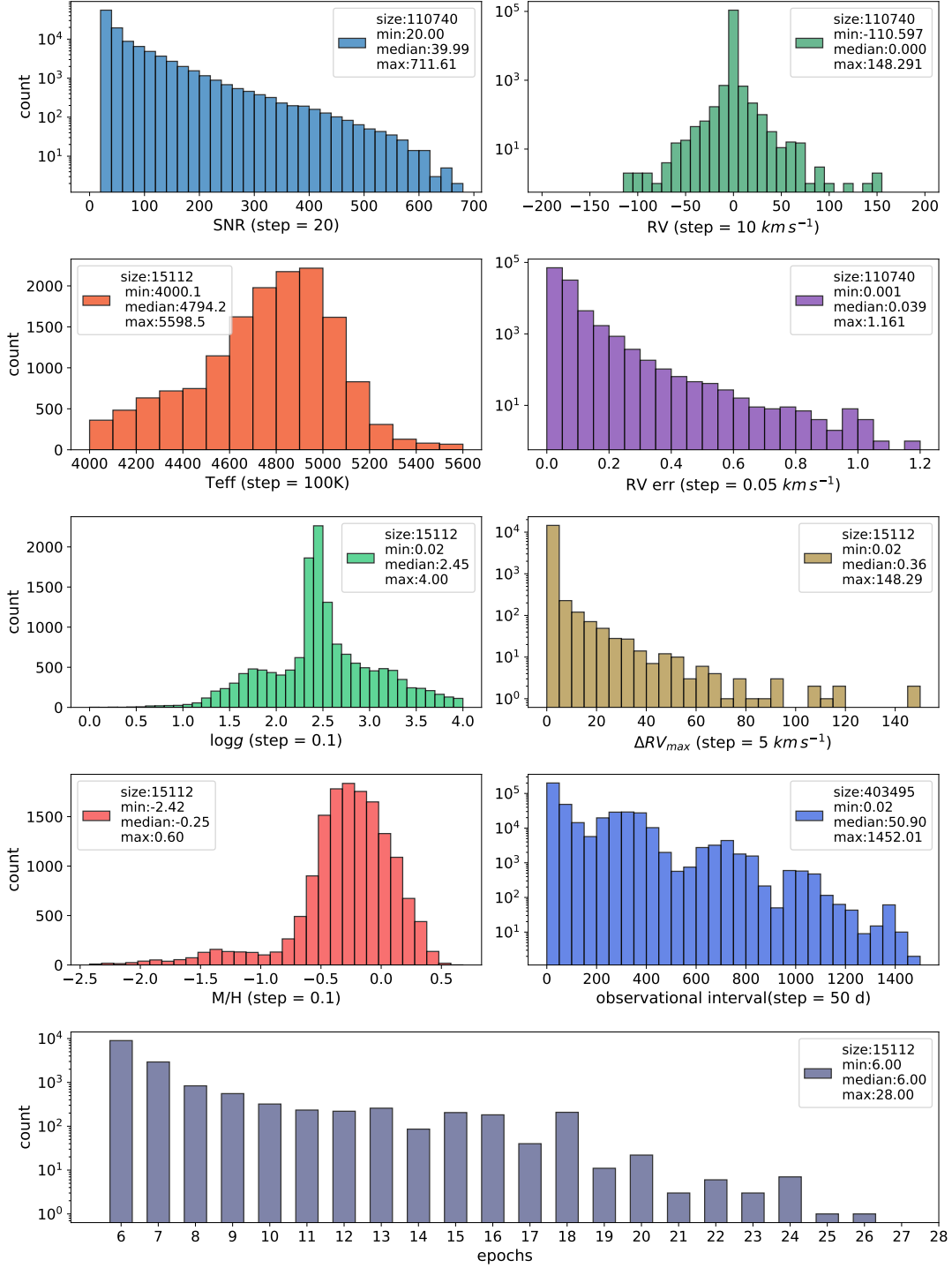


Figure 9. Basic information of the selected red giant samples.

in accordance with $\log g$ by using the equation 9.

$$P = \left(\frac{4\pi^2 R^3}{Gm_1(1+q)} \right)^{\frac{1}{2}}, R = \sqrt{\frac{Gm_1}{10^{\log g}}}. \quad (9)$$

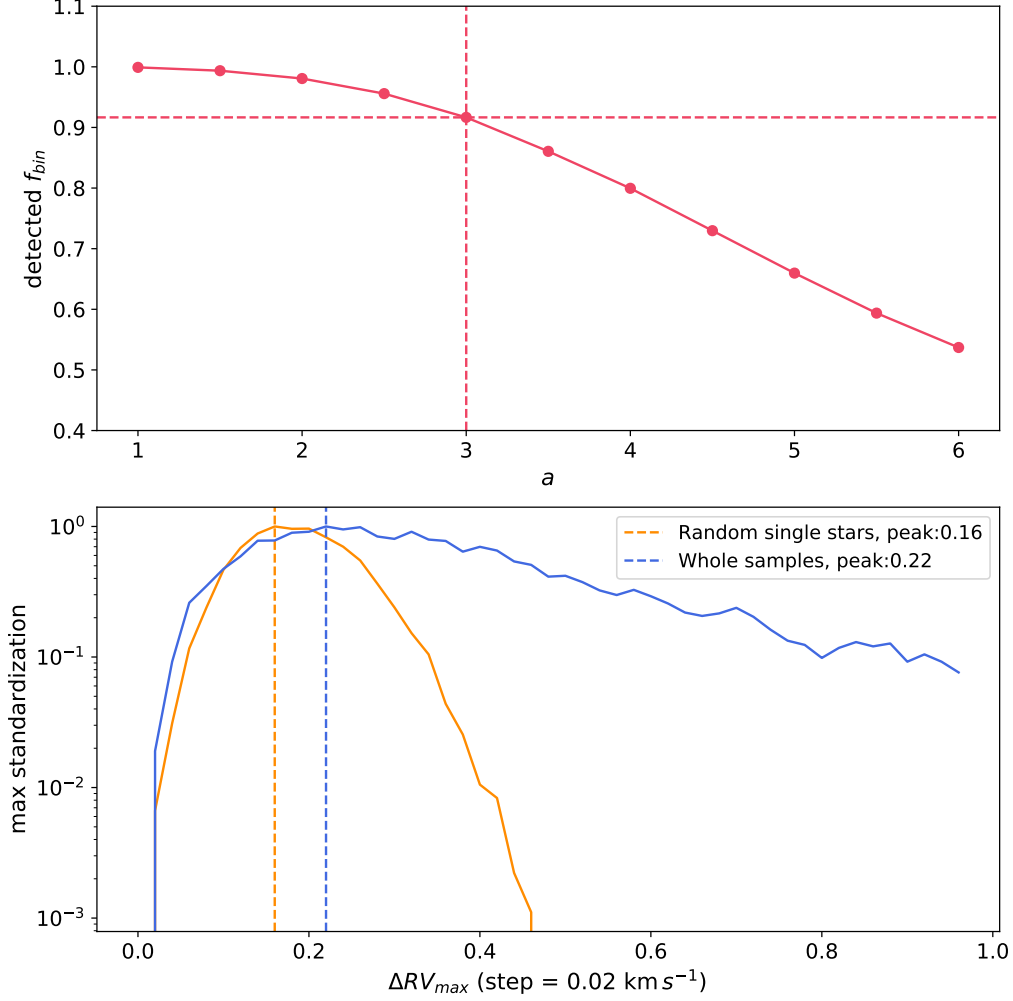


Figure 10. Estimating the error of RV through generations of single star samples with different ε .

Estimates of the lower limits of P for samples whose $0 < \log g < 1.8$ is 41.39 (days), $1.8 < \log g < 2.2$ is 7.07, $2.8 < \log g < 4.3$ is 1.5. These minima of P will be adopted in the subsequent Monte-Carlo simulations.

4.4. Samples that mimic the real data

We got 1959 sources' primary masses by cross-matching with the star catalogue published by Ness et al. (2016). In the MCMC simulations we randomly draw m_1 evenly from these 1959 masses to generate the mock samples using Equation 1. From Figure 9 we can see the maximum of the observation interval that between any pairs of observations is about 1452 days. That means we can not detect the binaries with orbital periods longer than 1452 days from these RGB data. Then the upper limit of the detected range of P was determined as 1400 days. Except m_1 and P , the detection ranges of other parameters were defined as the same as Table 2

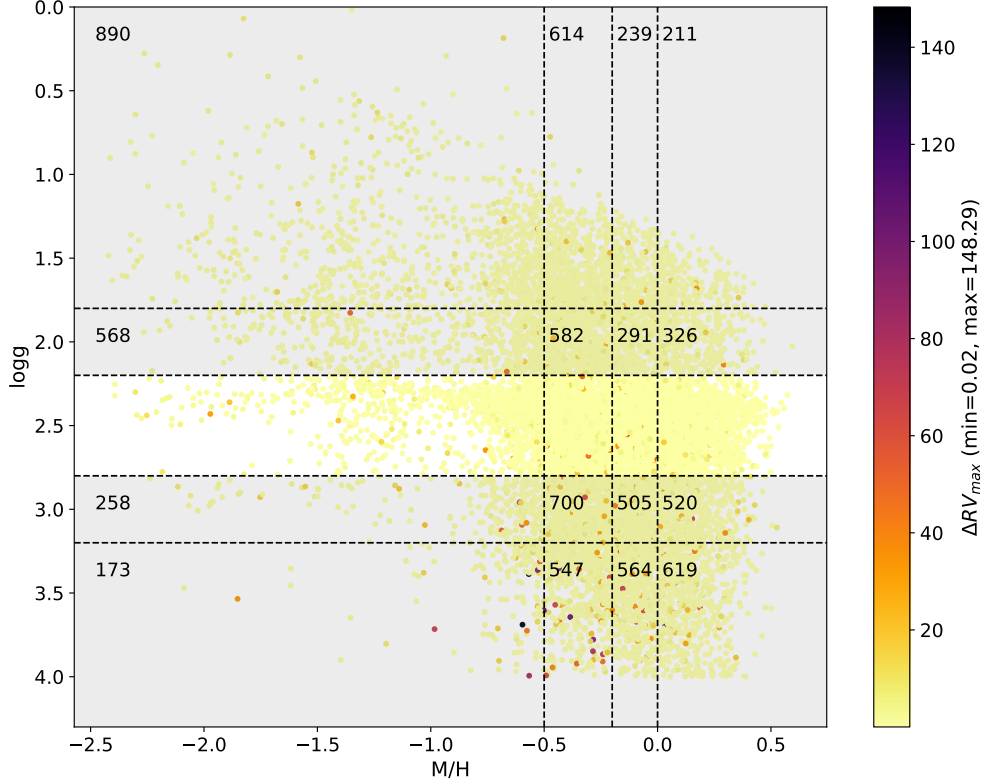


Figure 11. Meshes according M/H and $\log g$, the number in each block is the amount of observational sources included in which.

We generate 135 mock data groups with different combinations of sample size, epochs, π and f_{bin} as depicted in Figure 13. The minimum and maximum of orbital periods in these groups were 1.5 and 1400 days. The green, red and blue lines in the figure represent the true value of $\pi = (-1.5, 0, 1.5)$, respectively. Each cross-point of two dotted lines indicated the true value position of a group of mock data. We can find that the estimates of f_{bin} were accurate in almost all cases. The predictions of π are not as accurate when $f_{bin} = 0.1$, regardless of the sample size and epochs. When $f_{bin} \geq 0.3$ the results are getting closer to their true values respectively. On the overall trend, the estimations of f_{bin} are more stable and accurate than π . π will gain better constraints when the basic data is getting more sufficient.

4.5. Results

We calculated all the 16 subsets of real data displayed as Figure 11. The detection range of π was $[-2, 2]$ with step 0.1, f_{bin} was $[0, 1]$ with step 0.01. The results of π and f_{bin} with $\log g$ and M/H are displayed in Figure 14. Points in each error bar were peak positions. The lower and upper limits of error bars and the 15th and 85th percentiles. Lengths of error bars were defined as the half value of difference between the 15th and 85th percentiles, so there some upper limits of π were beyond over the detection range.

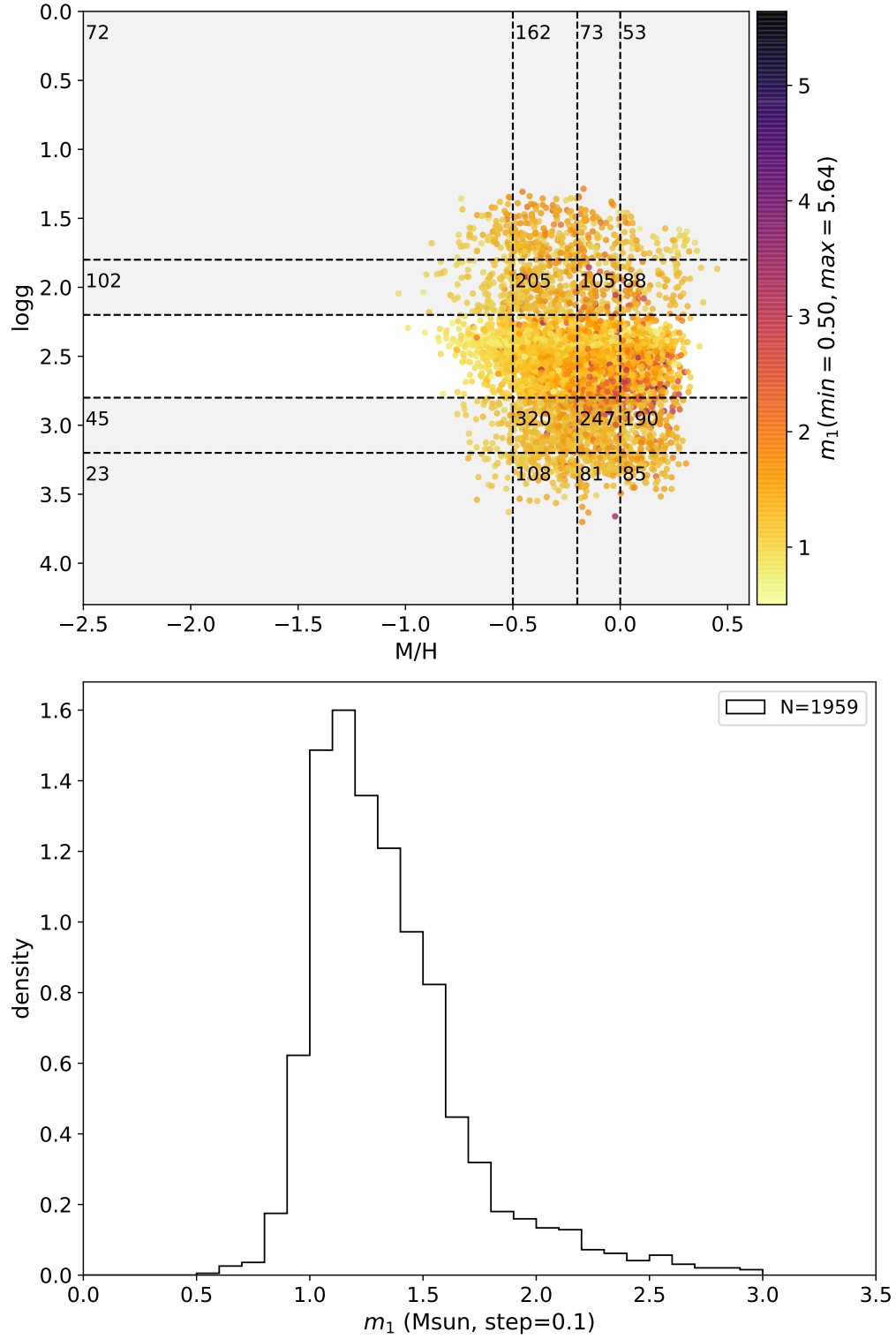


Figure 12. The obtained 1959 primary masses from [Ness et al. \(2016\)](#)

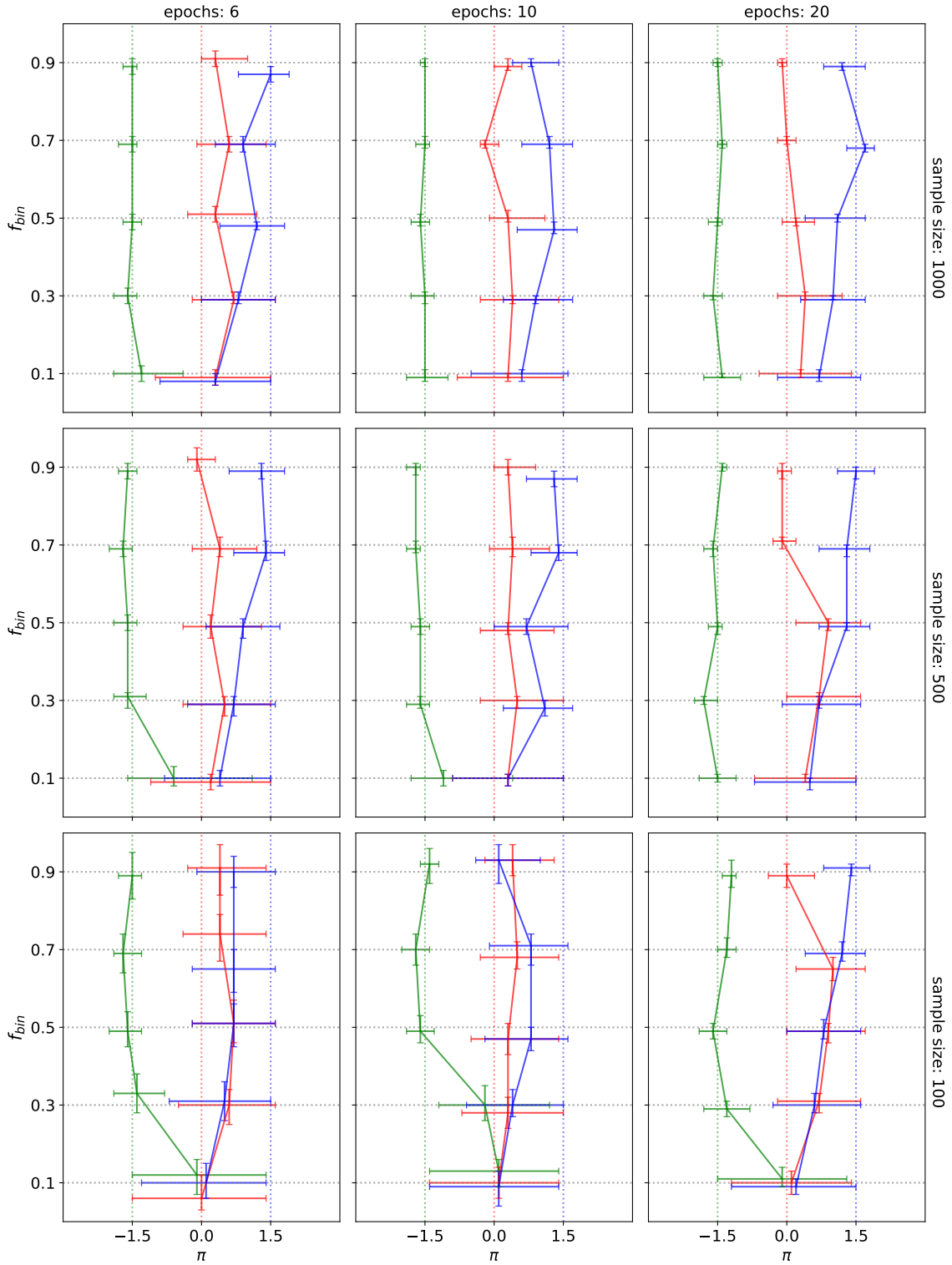


Figure 13. Simulated experiments with random samples that mimic the real data. Each cross-point of two dotted lines indicated the true value position of a group of mock data. Green, red and blue lines represent the true π of -1.5, 0, 1.5, respectively.

From the figure we can find that π were not change obviously with $\log g$ and M/H , error bars of which also wide especially when the corresponding f_{bin} is small. According to the above-mentioned simulations, we need more data to get precise predictions of π but the f_{bin} results were trusty. The max f_{bin} is about 0.45 when $3.2 \leq \log g < 4.3$ and $-2.5 \leq M/H < -0.5$, and min about 0.05 when $1.8 \leq \log g < 2.2$ and $0.0 \leq M/H < 0.6$. Generally, The f_{bin} estimations appeared a tendency of decreasing with the decrease of $\log g$ and decreasing with the increase of M/H .

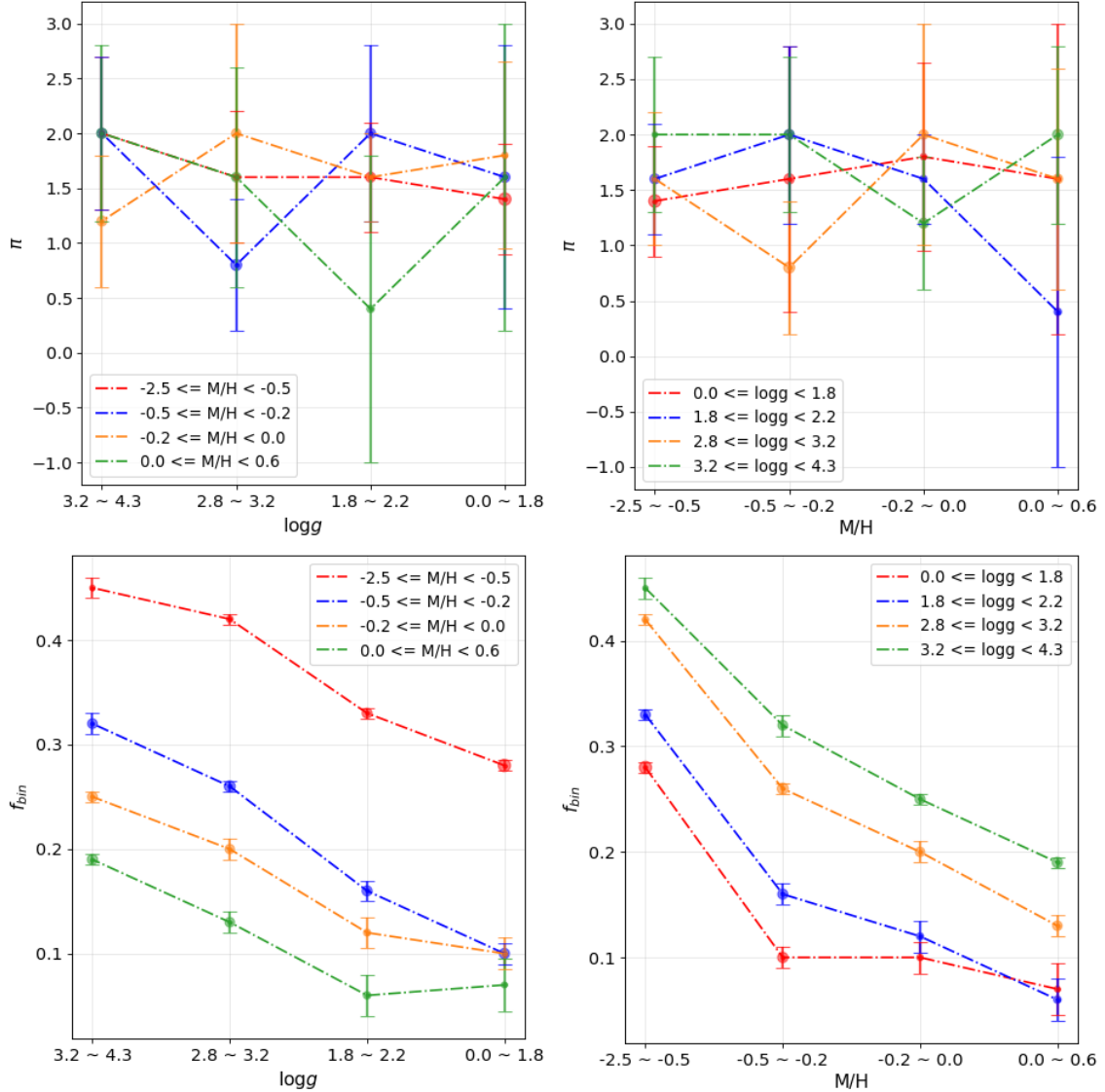


Figure 14. Estimating the error of RV through generations of single star samples with different ε .

5. DISCUSSION AND CONCLUSION

5.1. The tendency of f_{bin}

The trend of f_{bin} decreasing with $\log g$ (Figure 14) in red giants implies that some binary systems may be destroyed in the evolutionary processes or the primary would leave the RGB area in HRD (Hertzsprung–Russell diagram), or for other reasons.

For one thing, during the inflation of primary stars, the orbital angular momentum may be converted into the rotational angular momentum of which (Sepinsky et al. 2011; Gerosa et al. 2015; Zhang et al. 2009b,a; Greenhill et al. 1999; Namboodiri & Kochhar 1990; Wilson & Stothers 1975). The separation between the two components will get smaller and smaller. There is a certain probability that RLOF (Roche Lobe OverFlow)(King & Done 1993; Gies 2012; Vigna-Gómez et al. 2020) or CE (Common Envelop) will occur (Schreier et al. 2021; Jiang et al. 2021; Berzin et al. 2021). Finally, if the two stars merge into a single star, the binary system is devastated (Ivanova & Podsiadlowski 2002; Exter 2010; Jermyn & Cantiello 2020; Nakauchi et al. 2020).

For another thing, if there is a non-negligible mass loss in a binary system (Sana 2022; Pejcha et al. 2021; Ekström 2021; Doikov & Yushchenko 2021; Farrell et al. 2020; Brinkman et al. 2019; Evans et al. 2018) by stellar winds no matter from the primary or the secondary, the separation of the two components will get longer and longer as well as the orbital period. The RV variation of this kind of binary systems becomes less and less visible until we can not detect them. Binary calculated models based on radial velocities will regard these binaries as single stars, and result in the decrease of f_{bin} .

The above analysis of the f_{bin} tendency is from a statistical point of view. Evidence of how this trend arose requires further research.

5.2. *The DVCD method*

We proposed a new method DVCD for binary statistical research. This algorithm reduces the subjective component in preprocessing the original data and resolves two potential problems in previous methods. The experimental results show that the DVCD algorithm has reliable accuracy. When there is insufficient original data for us to get accurate predictions of orbital period distributions, the f_{bin} results are still accurate. Meanwhile, in one of our simulated experiments under the same hardware and software environments, the calculation time of the S13 method is about 74 hours but 29 33 seconds of DVCD. The running efficiency was about 10^4 times higher than the S13 method and about 10^5 higher than HBM. Nevertheless, DVCD was directly inspired by the work of its predecessors, particularly S13 and HBM.

Some red giants samples selected from APOGEE DR16 were analyzed by DVCD and statistical results were obtained. Although the f_{bin} tendency consisted of the above theoretical analysis, the results require multiparty authentication. Particularly, the observations of “star by star” are very helpful in demonstrating this phenomenon.

REFERENCES

- | | |
|--|---|
| <p>Aldoretta, E. J., Caballero-Nieves, S. M.,
Gies, D. R., et al. 2015, AJ, 149, 26,
doi: 10.1088/0004-6256/149/1/26</p> | <p>Berzin, E., Secunda, A., Cen, R.,
Menegas, A., & Göteborg, Y. 2021, APJ,
918, 5, doi: 10.3847/1538-4357/ac0af6</p> |
|--|---|

- Blondin, S., Bravo, E., Timmes, F., Dessart, L., & Hillier, D. J. 2021, arXiv e-prints, arXiv:2109.13840.
<https://arxiv.org/abs/2109.13840>
- Brinkman, H. E., Doherty, C. L., Pols, O. R., et al. 2019, *ApJ*, 884, 38, doi: [10.3847/1538-4357/ab40ae](https://doi.org/10.3847/1538-4357/ab40ae)
- Callister, T. A. 2021, PhD thesis, California Institute of Technology
- Chini, R., Hoffmeister, V. H., Nasserri, A., Stahl, O., & Zinnecker, H. 2012, *MNRAS*, 424, 1925, doi: [10.1111/j.1365-2966.2012.21317.x](https://doi.org/10.1111/j.1365-2966.2012.21317.x)
- Doikov, D. N., & Yushchenko, A. V. 2021, *Odessa Astronomical Publications*, 34, 40, doi: [10.18524/1810-4215.2021.34.244285](https://doi.org/10.18524/1810-4215.2021.34.244285)
- Dubey, R. K., & Pathak, S. D. 2021, in *Posters from the TESS Science Conference II (TSC2)*, 28, doi: [10.5281/zenodo.5121138](https://doi.org/10.5281/zenodo.5121138)
- Dunstall, P. R., Dufton, P. L., Sana, H., et al. 2015, *AA*, 580, A93, doi: [10.1051/0004-6361/201526192](https://doi.org/10.1051/0004-6361/201526192)
- Ekström, S. 2021, *Frontiers in Astronomy and Space Sciences*, 8, 53, doi: [10.3389/fspas.2021.617765](https://doi.org/10.3389/fspas.2021.617765)
- Evans, N. R., Karovska, M., Bond, H. E., et al. 2018, *ApJ*, 863, 187, doi: [10.3847/1538-4357/aad410](https://doi.org/10.3847/1538-4357/aad410)
- Exter, K. 2010, *GT1_kextexr_1: V838 Mon: aftermath of a stellar merger*, Herschel Space Observatory Proposal
- Farrell, E. J., Groh, J. H., Meynet, G., et al. 2020, *MNRAS*, 495, 4659, doi: [10.1093/mnras/staa1360](https://doi.org/10.1093/mnras/staa1360)
- Gao, S., Liu, C., Zhang, X., et al. 2014, *APJL*, 788, L37, doi: [10.1088/2041-8205/788/2/L37](https://doi.org/10.1088/2041-8205/788/2/L37)
- Gao, S., Zhao, H., Yang, H., & Gao, R. 2017, *MNRAS*, 469, L68, doi: [10.1093/mnrasl/slx048](https://doi.org/10.1093/mnrasl/slx048)
- García, F., Karpouzas, K., Méndez, M., et al. 2022, *MNRAS*, 513, 4196, doi: [10.1093/mnras/stac1202](https://doi.org/10.1093/mnras/stac1202)
- Ge, H., Webbink, R. F., Chen, X., & Han, Z. 2015, *ApJ*, 812, 40, doi: [10.1088/0004-637X/812/1/40](https://doi.org/10.1088/0004-637X/812/1/40)
- Gerosa, D., Veronesi, B., Lodato, G., & Rosotti, G. 2015, *MNRAS*, 451, 3941, doi: [10.1093/mnras/stv1214](https://doi.org/10.1093/mnras/stv1214)
- Gies, D. R. 2012, in *Astronomical Society of the Pacific Conference Series*, Vol. 465, *Proceedings of a Scientific Meeting in Honor of Anthony F. J. Moffat*, ed. L. Drissen, C. Robert, N. St-Louis, & A. F. J. Moffat, 275
- Gies, D. R., Lester, K. V., Wang, L., et al. 2020, *APJ*, 902, 25, doi: [10.3847/1538-4357/abb372](https://doi.org/10.3847/1538-4357/abb372)
- Greenhill, J. G., Galloway, D. K., & Murray, J. R. 1999, *PASA*, 16, 240, doi: [10.1071/AS99240](https://doi.org/10.1071/AS99240)
- Guo, Y., Li, J., Xiong, J., et al. 2021, arXiv e-prints, arXiv:2109.09775.
<https://arxiv.org/abs/2109.09775>
- Hilditch, R. W. 2001, *An Introduction to Close Binary Stars*
- Isi, M., Farr, W. M., Giesler, M., Scheel, M. A., & Teukolsky, S. A. 2021, *PRL*, 127, 011103, doi: [10.1103/PhysRevLett.127.011103](https://doi.org/10.1103/PhysRevLett.127.011103)
- Ivanova, N., & Podsiadlowski, P. 2002, *apss*, 281, 191, doi: [10.1023/A:1019553109023](https://doi.org/10.1023/A:1019553109023)
- Jermyn, A. S., & Cantiello, M. 2020, *apj*, 900, 113, doi: [10.3847/1538-4357/ab9e70](https://doi.org/10.3847/1538-4357/ab9e70)
- Jiang, L., Tauris, T. M., Chen, W.-C., & Fuller, J. 2021, *APJL*, 920, L36, doi: [10.3847/2041-8213/ac2cc9](https://doi.org/10.3847/2041-8213/ac2cc9)
- Kangas, T., Portinari, L., Mattila, S., et al. 2017, *A&A*, 597, A92, doi: [10.1051/0004-6361/201628705](https://doi.org/10.1051/0004-6361/201628705)
- Karino, S. 2022, *MNRAS*, 514, 191, doi: [10.1093/mnras/stac1334](https://doi.org/10.1093/mnras/stac1334)
- Khoshnood, R. S., Teymouri, M., Hatami, E., & Balanezhad, A. Z. 2015, *Russian Journal of Physical Chemistry A*, 89, 1560, doi: [10.1134/S0036024415090265](https://doi.org/10.1134/S0036024415090265)
- King, A. R., & Done, C. 1993, *mnras*, 264, 388, doi: [10.1093/mnras/264.2.388](https://doi.org/10.1093/mnras/264.2.388)
- Kobulnicky, H. A., Kiminki, D. C., Lundquist, M. J., et al. 2014, *APJS*, 213, 34, doi: [10.1088/0067-0049/213/2/34](https://doi.org/10.1088/0067-0049/213/2/34)

- Lee, C.-H., & Lin, C.-C. 2017, *Research in Astronomy and Astrophysics*, 17, 15, doi: [10.1088/1674-4527/17/2/15](https://doi.org/10.1088/1674-4527/17/2/15)
- Liao, S., Qi, Z., Cao, Z., & Tang, Z. 2021, *PASP*, 133, 024501, doi: [10.1088/1538-3873/abd4bd](https://doi.org/10.1088/1538-3873/abd4bd)
- Liu, C., Deng, L.-C., Carlin, J. L., et al. 2014, *APJ*, 790, 110, doi: [10.1088/0004-637X/790/2/110](https://doi.org/10.1088/0004-637X/790/2/110)
- Lomax, J. R., Fullard, A. G., Malatesta, M. A., et al. 2017, *MNRAS*, 464, 1936, doi: [10.1093/mnras/stw2457](https://doi.org/10.1093/mnras/stw2457)
- Lu, Y., Li, X. R., Lin, Y. T., & Qiu, K. B. 2018, *Acta Astronomica Sinica*, 59, 35
- Lu, Y., Li, X.-r., Lin, Y.-t., & Qiu, K.-b. 2019, *ChA&A*, 43, 237, doi: [10.1016/j.chinastron.2019.04.006](https://doi.org/10.1016/j.chinastron.2019.04.006)
- Luo, F., Zhao, Y.-H., Li, J., Guo, Y.-J., & Liu, C. 2021, arXiv e-prints, arXiv:2108.11120, <https://arxiv.org/abs/2108.11120>
- Lynch, R., Vitale, S., Essick, R., Katsavounidis, E., & Robinet, F. 2015, arXiv e-prints, arXiv:1511.05955, <https://arxiv.org/abs/1511.05955>
- Mazzola, C. N., Badenes, C., Moe, M., et al. 2020, *MNRAS*, 499, 1607, doi: [10.1093/mnras/staa2859](https://doi.org/10.1093/mnras/staa2859)
- Nakauchi, D., Inayoshi, K., & Omukai, K. 2020, *apj*, 902, 81, doi: [10.3847/1538-4357/abb463](https://doi.org/10.3847/1538-4357/abb463)
- Namboodiri, P. M. S., & Kochhar, R. K. 1990, in *NASA Conference Publication*, Vol. 3098, NASA Conference Publication, ed. J. W. Sulentic, W. C. Keel, & C. M. Telesco, 589–593
- Ness, M., Hogg, D. W., Rix, H. W., et al. 2016, *APJ*, 823, 114, doi: [10.3847/0004-637X/823/2/114](https://doi.org/10.3847/0004-637X/823/2/114)
- Pejcha, O., Metzger, B. D., Tyles, J. G., & Tomida, K. 2021, *ApJ*, 922, 273, doi: [10.3847/1538-4357/ac3764](https://doi.org/10.3847/1538-4357/ac3764)
- Peters, G. 2011, *Accretion Structures in Algol-Type Interacting Binary Systems*, NASA Proposal id.11-ADAP11-269
- Price-Whelan, A. M., Hogg, D. W., Rix, H.-W., et al. 2018, *AJ*, 156, 18, doi: [10.3847/1538-3881/aac387](https://doi.org/10.3847/1538-3881/aac387)
- Raghavan, D., McAlister, H. A., Henry, T. J., et al. 2010, *APJS*, 190, 1, doi: [10.1088/0067-0049/190/1/1](https://doi.org/10.1088/0067-0049/190/1/1)
- Sana, H. 2022, arXiv e-prints, arXiv:2203.16332, <https://arxiv.org/abs/2203.16332>
- Sana, H., de Mink, S. E., de Koter, A., et al. 2012, *Science*, 337, 444, doi: [10.1126/science.1223344](https://doi.org/10.1126/science.1223344)
- Sana, H., de Koter, A., de Mink, S. E., et al. 2013, *AA*, 550, A107, doi: [10.1051/0004-6361/201219621](https://doi.org/10.1051/0004-6361/201219621)
- Saz Parkinson, P. M., Xu, H., Yu, P. L. H., et al. 2016, *ApJ*, 820, 8, doi: [10.3847/0004-637X/820/1/8](https://doi.org/10.3847/0004-637X/820/1/8)
- Schreier, R., Hillel, S., Shiber, S., & Soker, N. 2021, *MNRAS*, 508, 2386, doi: [10.1093/mnras/stab2687](https://doi.org/10.1093/mnras/stab2687)
- Sepinsky, J. F., Willems, B., & Kalogera, V. 2011, in *American Astronomical Society Meeting Abstracts*, Vol. 217, American Astronomical Society Meeting Abstracts #217, 105.04
- Shao, Y., & Li, X.-D. 2018, *ApJ*, 867, 124, doi: [10.3847/1538-4357/aae648](https://doi.org/10.3847/1538-4357/aae648)
- Shapiro, S. 2016, *Compact Binary Mergers in General Relativity*, NASA ATP Proposal
- Shin, J., Woo, J.-H., Kim, M., & Wang, J. 2021, *ApJ*, 908, 81, doi: [10.3847/1538-4357/abd779](https://doi.org/10.3847/1538-4357/abd779)
- Sota, A., Maíz Apellániz, J., Morrell, N. I., et al. 2014, *APJS*, 211, 10, doi: [10.1088/0067-0049/211/1/10](https://doi.org/10.1088/0067-0049/211/1/10)
- Spera, M., Giacobbo, N., & Mapelli, M. 2016, *MemSAI*, 87, 575, <https://arxiv.org/abs/1606.03349>
- Tian, Z.-J., Liu, X.-W., Yuan, H.-B., et al. 2018, *Research in Astronomy and Astrophysics*, 18, 052, doi: [10.1088/1674-4527/18/5/52](https://doi.org/10.1088/1674-4527/18/5/52)
- Troup, N. W., Nidever, D. L., De Lee, N., et al. 2016, *AJ*, 151, 85, doi: [10.3847/0004-6256/151/3/85](https://doi.org/10.3847/0004-6256/151/3/85)
- Tsebrenko, D., & Soker, N. 2015, *MNRAS*, 447, 2568, doi: [10.1093/mnras/stu2567](https://doi.org/10.1093/mnras/stu2567)
- van Kooten, M. A. M., Kenworthy, M., & Doelman, N. 2020, *MNRAS*, 499, 2817, doi: [10.1093/mnras/staa3048](https://doi.org/10.1093/mnras/staa3048)

- Vigna-Gómez, A., MacLeod, M., Neijssel, C. J., et al. 2020, *pasa*, 37, e038, doi: [10.1017/pasa.2020.31](https://doi.org/10.1017/pasa.2020.31)
- Wang, S., Kawai, N., Shidatsu, M., et al. 2022, *MNRAS*, doi: [10.1093/mnras/stac1503](https://doi.org/10.1093/mnras/stac1503)
- Wilson, R. E., & Stothers, R. 1975, *MNRAS*, 170, 497, doi: [10.1093/mnras/170.3.497](https://doi.org/10.1093/mnras/170.3.497)
- Zhang, J., Qian, S. B., & Boonrucksar Soobthornthum. 2009a, *Acta Astronomica Sinica*, 50, 29
- Zhang, J., Qian, S.-B., & Soobthornthum, B. 2009b, *Research in Astronomy and Astrophysics*, 9, 307, doi: [10.1088/1674-4527/9/3/005](https://doi.org/10.1088/1674-4527/9/3/005)
- Zhang, W.-L., Yi, S.-X., Yang, Y.-P., & Qin, Y. 2022, *Research in Astronomy and Astrophysics*, 22, 065012, doi: [10.1088/1674-4527/ac6aac](https://doi.org/10.1088/1674-4527/ac6aac)
- Zheng, Y.-L., & Shen, S.-Y. 2020a, *ApJS*, 248, 22, doi: [10.3847/1538-4365/ab8acb](https://doi.org/10.3847/1538-4365/ab8acb)
- . 2020b, *ApJS*, 246, 12, doi: [10.3847/1538-4365/ab5c26](https://doi.org/10.3847/1538-4365/ab5c26)
- . 2021, *ApJ*, 911, 105, doi: [10.3847/1538-4357/abeaa2](https://doi.org/10.3847/1538-4357/abeaa2)
- Ziegerer, E., Heber, U., Geier, S., et al. 2017, *A&A*, 601, A58, doi: [10.1051/0004-6361/201730437](https://doi.org/10.1051/0004-6361/201730437)